# The effect of Ti(CN)/TiNb(CN) coating on erosion–corrosion resistance

## Efecto del recubrimiento de Ti(CN)/TiNb(CN) sobre la resistencia a la corrosión–erosión

W. Aperador[1], C. Ramírez[2], J. C. Caicedo[3]

**ABSTRACT**

The goal of this work was to study electrochemical behaviour in corrosion-erosion conditions for Ti(CN)/TiNb(CN) multilayer coatings having 1, 50, 100, 150 and 200 bilayer periods on AISI 4140 steel substrates by using a multi-target magnetron reactive sputtering device, with an r.f. source (13.56 MHz), two cylindrical magnetron cathodes and two stoichiometric TiC and Nb targets. The multilayers were evaluated by comparing them to corrosion, erosion and erosion corrosion for a 30º impact angle in a solution of 0.5 M NaCl and silica, analysing the effect of impact angle and the number of bilayers on these coatings' corrosion resistance. The electrochemical characterisation was performed using electrochemical impedance spectroscopy for analysing corrosion surface; surface morphology was characterised by using a high-resolution scanning electron microscope (SEM). The results showed a decreased corrosion rate for multilayer systems tested at 30°.

**Keywords:** Multilayer, dynamic corrosion, corrosion-erosion, erosion, scanning electron microscope.

**RESUMEN**

El objetivo de este trabajo es el de estudiar el comportamiento electroquímico bajo condiciones de corrosión-erosión a los recubrimientos multicapas de Ti(CN)/TiNb(CN) con periodos de 1, 50, 100, 150 y 200 bicapas depositadas en sustratos de acero AISI 4140, mediante un sistema magnetrón sputtering con r.f reactivo (13.56 MHz) y dos cátodos cilíndricos con estequiometría de los blancos de TiC y Nb. Las multicapas se evaluaron al comparar la corrosión, la erosión y la corrosión-erosión para un ángulo de impacto de 30° en una solución de 0,5 M NaCl y sílice, y al analizar el efecto del ángulo de impacto y el número de bicapas en función de la resistencia a la corrosión. La caracterización electroquímica se realizó mediante la técnica de espectroscopia de impedancia electroquímica para evaluar el proceso de corrosión en la superficie; la morfología superficial se caracterizó con la utilización de un microscopio electrónico de barrido (SEM). Los resultados muestran una disminución en la tasa de corrosión para los sistemas multicapa ensayada a 30°.

**Palabras clave:** multicapas, corrosión dinámica, corrosión-erosión, erosión, microscopia electrónica de barrido.

**Received: March 12th 2012**
**Accepted: July 16th 2012**

## Introduction

Erosion-corrosion is an accelerated corrosion of metals due to a combination of chemical attack and abrasion by the physical movement of fluids containing suspended solids. Alloys forming a film surface in a corrosive environment usually have a corrosion speed limit above which corrosion becomes rapidly accelerated. Erosion-corrosion is associated with current induced by the mechanical removal of the protective film from the surface thereby resulting in a further increase of corrosion rate for chemical or electrochemical processes. Surface engineering of metal substrates having protective film attracts unanimous attention from industry and researchers as it produces a host of properties, such as wear and erosion resistance, and oxidation and corrosion resistance. However, a coating is highly functional only if the interface between the film and the substrate is sound and strong (Aperador, *et al*., 2010; Caicedo, *et al*., 2011; Aperador, *et al*., 2011).

Much research in recent years has been aimed at developing multilayered structures having nanometric period thickness (also called superlattices) for their use as protective hard coatings. Such structures' appeal lies in their improved mechanical and tribological properties, compared to those of their individual components (Romero, *et al*., 2004; Holmberg, *et al*., 1988; Koehler, 1970; Junhua, *et al*., 2000; Philip, *et al*., 1999; Helmersson, *et al*., 1987). Hardness enhancement in thin film isostructural superlattices have been successfully modelled by dislocation image force theories, arising from Koehler's first model (Shtansky,

[1] William Aperador Chaparro. Affiliation: Universidad Militar Nueva Granada, Colombia. PhD in Material Engineering, Universidad del Valle, Colombia. MSc. in Metallurgy and Material Science, BSc. in Physics, Universidad Pedagogica y Tecnológica de Colombia. E-mail: g.ing.materiales@gmail.com
[2] Carlos Ramírez Martín. Affiliation: Universidad de Boyacá, Colombia. MSc. in Metallurgy and Material Science, BSc. in Physics, Universidad Pedagogica y Tecnológica de Colombia. E-mail: cramirezm@uniboyaca.edu.co
[3] Julio Cesar Caicedo. Affiliation: Universidad del Valle, Colombia. PhD. in Material Engineering, BSc. in Material Engineering, Universidad del Valle, Colombia. E-mail: jcaicedo@gmail.com

**How to cite:** Aperador W., Ramírez C., Caicedo J. C. (2012). The effect of Ti(CN)/TiNb(CN) coating on erosion–corrosion resistance. Ingeniería e Investigación. Vol. 32, No. 2, August 2012, pp. 6-11.

2004) based on shear moduli differences, in combination with Chu and Barnett's correction assuming dislocation propagation inside monolayers (Caicedo, *et al.*, 2010). There have also been reports of mechanical and electrochemical enhancement in isostructural superlattices (Barshilia, *et al.*, 2007; Barshilia, *et al.*, 2009; Jehn, 2000). Amongst such isostructural systems, metal/ceramic and ceramic/ceramic superlattices have been receiving greater attention since this combination can exhibit high hardness values, often increasing it by more than 100% over rule of mixtures, while retaining good ductility and high anticorrosive properties. Several metal/ceramic and ceramic/ceramic superlattices have been studied during the past 10 years including Ti/TiN (Barshilia, *et al.*, 2007), TiN/V0.3Nb0.7N (Barshilia, *et al.*, 2009) or the TiN/NbN (Jehn, 2000). Nitride coatings, which are characterised by high hardness, wear resistance and corrosion resistance, are finding ever wider use for strengthening and protecting construction steel from wear and corrosion. Their coating thickness which, in many cases does not exceed 5 μm, is a significant disadvantage limiting their use. In connection with this, broadening the use of physical vapour deposition (PVD) magnetron sputtering technology for strengthening machine parts is possible with the development of multilayer coatings having a higher combination of properties. Pore size and quantity is one of the most important parameters determining nitride coatings' service properties as they pierce it all the way through to the base, resulting in protective layer thinness and serving as origins for corrosion. It is known that PVD coatings have significantly less porosity compared to coatings obtained by other vacuum technology methods and also by gas thermal spraying methods. In some cases magnetron sputtering makes it possible to obtain porosity-free coatings, mainly in multilayers having 1 μm thickness, resulting from the high packing density of the atoms being concentrated. However, according to data in some works, nitride coating porosity may reach 5% which differs from the multilayer nitrides where porosity decreases to 1% (Jehn, 2000). Therefore, multilayer nitride coating corrosion resistance is higher than that of single-layer ones, which may be explained by their greater thickness and features of their microstructure, including the absence of circular crystals characteristic of single layer coatings; nitride coating failure exposed to the action of a corrosive medium occurs at structural defects, thereby determining their corrosion resistance and electrochemical properties (Shtansky, 2004). This work was aimed at studying the behaviour of 3 μm thickness Ti(CN)/TiNb(CN) multilayer coatings under corrosive-erosive fluid, regarding increasing the bilayer number or decreasing the bilayer period. This work also compared corrosion-erosion behaviour presented by the AISI 4140 steel uncoated substrate with all Ti(CN)/TiNb(CN) multilayered ones.

Erosion-corrosion is an accelerated corrosion of metals due to a combination of chemical attack and abrasion by the physical movement of fluids containing suspended solids. Alloys forming a film surface in a corrosive environment usually have a corrosion speed limit above which corrosion becomes rapidly accelerated. Erosion-corrosion is associated with current induced by the mechanical removal of the protective film from the surface thereby resulting in a further increase of corrosion rate for chemical or electrochemical processes. Surface engineering of metal substrates having protective film attracts unanimous attention from industry and researchers as it produces a host of properties, such as wear and erosion resistance, and oxidation and corrosion resistance. However, a coating is highly functional only if the interface between the film and the substrate is sound and strong (Aperador, *et al.*, 2010; Caicedo, *et al.*, 2011; Aperador, *et al.*, 2011).

Much research in recent years has been aimed at developing multilayered structures having nanometric period thickness (also called superlattices) for their use as protective hard coatings. Such structures' appeal lies in their improved mechanical and tribological properties, compared to those of their individual components (Romero, *et al.*, 2004; Holmberg, *et al.*, 1988; Koehler, 1970; Junhua, *et al.*, 2000; Philip, *et al.*, 1999; Helmersson, *et al.*, 1987). Hardness enhancement in thin film isostructural superlattices have been successfully modelled by dislocation image force theories, arising from Koehler's first model (Shtansky, 2004) based on shear moduli differences, in combination with Chu and Barnett's correction assuming dislocation propagation inside monolayers (Caicedo, *et al.*, 2010). There have also been reports of mechanical and electrochemical enhancement in isostructural superlattices (Barshilia, *et al.*, 2007; Barshilia, *et al.*, 2009; Jehn, 2000). Amongst such isostructural systems, metal/ceramic and ceramic/ceramic superlattices have been receiving greater attention since this combination can exhibit high hardness values, often increasing it by more than 100% over rule of mixtures, while retaining good ductility and high anticorrosive properties. Several metal/ceramic and ceramic/ceramic superlattices have been studied during the past 10 years including Ti/TiN (Barshilia, *et al.*, 2007), TiN/V0.3Nb0.7N (Barshilia, *et al.*, 2009) or the TiN/NbN (Jehn, 2000). Nitride coatings, which are characterised by high hardness, wear resistance and corrosion resistance, are finding ever wider use for strengthening and protecting construction steel from wear and corrosion. Their coating thickness which, in many cases does not exceed 5 μm, is a significant disadvantage limiting their use. In connection with this, broadening the use of physical vapour deposition (PVD) magnetron sputtering technology for strengthening machine parts is possible with the development of multilayer coatings having a higher combination of properties. Pore size and quantity is one of the most important parameters determining nitride coatings' service properties as they pierce it all the way through to the base, resulting in protective layer thinness and serving as origins for corrosion. It is known that PVD coatings have significantly less porosity compared to coatings obtained by other vacuum technology methods and also by gas thermal spraying methods. In some cases magnetron sputtering makes it possible to obtain porosity-free coatings, mainly in multilayers having 1 μm thickness, resulting from the high packing density of the atoms being concentrated. However, according to data in some works, nitride coating porosity may reach 5% which differs from the multilayer nitrides where porosity decreases to 1% (Jehn, 2000). Therefore, multilayer nitride coating corrosion resistance is higher than that of single-layer ones, which may be explained by their greater thickness and features of their microstructure, including the absence of circular crystals characteristic of single layer coatings; nitride coating failure exposed to the action of a corrosive medium occurs at structural defects, thereby determining their corrosion resistance and electrochemical properties (Shtansky, 2004). This work was aimed at studying the behaviour of 3 μm thickness Ti(CN)/TiNb(CN) multilayer coatings under corrosive-erosive fluid, regarding increasing the bilayer number or decreasing the bilayer period. This work also compared corrosion-erosion behaviour presented by the AISI 4140 steel uncoated substrate with all Ti(CN)/TiNb(CN) multilayered ones.

## Experimental details

Ti(CN)/TiNb(CN) multilayers were deposited on AISI 4140 steel substrates by using a multitarget magnetron reactive sputtering technique, with an r.f. source (13.56 MHz) and two stoichiometric TiC and Nb targets (99.9% purity for both targets). The

deposition parameters for obtaining high-quality coatings were 400 W sputtering power for TiC and 350 W for the Nb target, 300°C substrate temperature, 60 RPM circular rotation substrate , to facilitate stoichiometric quaternary film formation which is necessary for obtaining FCC crystal structure. The sputtering gas was a mixture of 76% Ar (50 sccm) and 24% N2 (16 sccm) with 6x10 3 mbar total working pressure. An unbalanced r.f. bias voltage gave -50 V constant voltage offset. Moreover, our magnetron sputtering device had a substrate positioning substrate system in relationship to target spot; this allowed varying bilayer number from 1, 50, 100, 150 and 200, changing the bilayer period. The deposited Ti(CN)/TiNb(CN) multilayers total thickness was measured by a Dektak 8000 profilometer with 12.00±0.04 µm tip diameter and 1000 µm–1200 µm scanning length. Thickness was 3.00 ± 0.04 µm for the sample of 200 bilayers.. Individual thickness varied regarding bilayer number from n = 1 to n = 200 producing layers having 1.5 µm to 15 nm thickness, respectively.

A device built for evaluating chemical attack on metallic materials and coated materials was used for analysing the erosive–corrosive effect. Figure 1 shows the erosive–corrosive test device consisting of a tribometer with a glass container for erosive–corrosive storage, a sample holder acrylic cover and impelling high ultra-molecular weight polyethylene (HUMWPE) electrodes resting on a Teflon shaft attached to the main shaft motor providing fluid motion. The container lid allowed locating sample exposure at 30° impact angle for corrosive fluid action, as well as the reference electrode and counter-electrode. The latter angle led to perpendicular sample location regarding fluid flow; fluid movement was caused by a shaft-driven motor. The tangential speed applied to the fluid with erosive particles was fixed at 13 m/s, this took into account that impeller radius was 0.055 m and motor speed was fixed at 2,250 RPM. The electrochemical study was carried out with a potentiostat (Gamry PCI4300) having Gamry framework (version 4.21/EIS 300 software), using electrochemical impedance spectroscopy (EIS). These curves were drawn at room temperature using a cell supporting one working electrode within an exposed area (1 cm2), a reference electrode (Ag/AgCl) and graphite counter electrode in a 0.5 M NaCl solution with distilled water. Resting potential was measured for 30 minutes. The electrolyte's electrochemical behaviour was studied by EIS at open circuit potential for 30 minutes to establish stable open circuit potential values at which the EIS measurements were initiated. Frequency sweeps were conducted for Nyquist diagrams in the 104 Hz to 10-3 Hz range using a sinusoidal voltage perturbation with 10 mV signal amplitude. Measurements were made on a set of three different replicate samples. In this work, silica (SiO2) was used as abrasive agent (210 µm to 300 µm particle size, 240 minute exposure time). This solution was chosen because it is used to study steel materials due to facilitating observation in the defined anodic region and chloride addition guaranteeing an effective attack. Surface morphology was characterised by analysing corrosion surface using a high-resolution scanning electron microscope (SEM) (Philips XL 30 FEG).

## Results and discussion

Figure 2 shows the Nyquist diagrams for the substratum and multilayer coatings, immersed in a 0.5 M NaCl solution and exposed to dynamic corrosion. These coatings had increased performance regarding total impedance in each multilayer tested, bilayers 100, 150 and 200 being the most prominent. The multilayer Nyquist diagrams showed capacitive behaviour at high frequencies in which a flattened semicircle was defined; this flattening of the semicircle was associated with frequency dispersion due to the fact that the electrode surface was not homogeneous. There was also diffusion which aimed to define a second semicircle at low frequencies (Orazem and Tribollet, 2008).

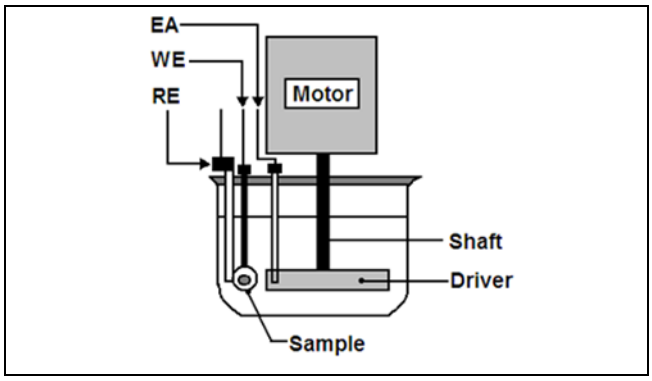


Figure 1. Diagram of f device used for corrosion–erosion wear testing. The acronyms EA, WE and RE in the figure represent auxiliary electrode, working electrode and reference electrode.

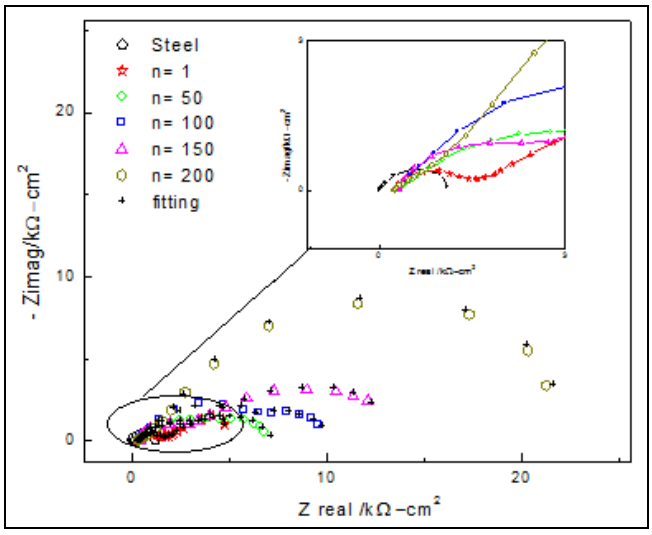


Figure 2. Impedance diagram of dynamic corrosion for hetero structures Ti(CN)/TiNb(CN) regarding the number of bilayers

Figure 2 also includes the results of a simulation using the electrical circuit shown in Figure 3b. As can be seen, there was good agreement between experimental and simulated results.

Table 1 shows the values for the parameters used in the simulation. Ohm resistance (RΩ) was the sum of electrolyte resistance and metal resistance RΩ = Rs + Rm. The impedance of a constant phase element (CPE) was expressed as ZCPE = (T(i•ω)φ)-1 where T and φ were CPE parameters. The CPE can be used to describe pure resistor (φ = 0, T = R -1), a pure capacitor (φ = 1, T= C), or a pure inductor (φ = -1, T = L-1). It was also associated with the Warburg element if φ = 0.5. Total impedance values were calculated theoretically and were equivalent to those in Table 1; also, the parameters used in the simulation were included, their values being obtained from a complex non-linear least squares (CNLS) algorithm. The CNLS method is one of the most common approaches for modelling impedance data. This is partially due to commercial fitting software like Zplot and LEVM which use the CNLS method. CNLS was used to fit the real and imaginary parts or the magnitude and experimental impedance or

admittance phase data to an equivalent circuit or a rational function.

Figure 3 shows the equivalent circuit corresponding to the Nyquist diagrams for coatings, displaying a capacitance called "constant phase element" (CPE) which was independent of faradic reactions, in turn, contributing to pseudo-capacitance (CPE2 + CPE1) of total system impedance. Moreover, there was also electrical resistance associated with electrolyte resistance (Rs) in this electrochemical cell, which in turn would become manifest in total system impedance. The values for α (Table 1) corresponded to the exponential coefficient of the shift of the phase's angle (π/2); the values of α for the coatings and the substratum for the CPE in high frequency values ranged from 0.70 to 0.87, indicating that surface roughness generated a distribution of the load. The CPE at low frequencies had a 0.70 value for α for one bilayer and 0.72 for 50 bilayers, indicating species migration or diffusion; for 100, 150 and 200 bilayers, the values of α were 0.82, 0.79 and 0.84, generating charge carrier density distribution, i.e. a double-layer having a complex structure.

Table 1. Comparing experimental data for the dynamic substratum corrosion and coating system to bias variation and the results obtained by Kramers–Kronig relationships (adjustment)

| | $R_\Omega$ $\Omega\,cm^2$ | $CPE_1$ $\mu F\ cm^{-2}\ s^{-(1-\alpha 1)}$ | $\alpha_1$ | $R_1$ $10^3$ $\Omega\,cm^2$ | $CPE_2$ $\mu F\ cm^{-2}\ s^{-(1-\alpha 2)}$ | $\alpha_2$ | $R_2$ $10^3$ $\Omega\,cm^2$ |
|---|---|---|---|---|---|---|---|
| **n=200** | 43.53 (0.3%) | 17.46 (1.7%) | 0.87 (0.2%) | 8.18 (3%) | 64.23 (3%) | 0.84 (0.2%) | 19.11 (5%) |
| **n=150** | 38.1 (0.2%) | 10.44 (2.1%) | 0.73 (0.4%) | 6.10 (3%) | 22.32 (3%) | 0.79 (0.2%) | 12.43 (4%) |
| **n=100** | 38.6 (0.3%) | 7.65 (1.9%) | 0.70 (0.6%) | 4.31 (2%) | 16.43 (2.5%) | 0.82 (0.3%) | 8.35 (3%) |
| **n=50** | 43.2 (0.4%) | 5.79 (2.3%) | 0.81 (0.4%) | 3.02 (4%) | 10.65 (2.4%) | 0.72 (0.4%) | 5.81 (4%) |
| **n=1** | 38.2 (0.2%) | 4.65 (1.7%) | 0.82 (0.3%) | 2.15 (3%) | 7.34 (2.1%) | 0.70 (1.4%) | 4.43 (5%) |
| **Steel** | 34.1 (0.4%) | 3.45 (3.1%) | 0.71 (0.4%) | 1.61 3%) | | | |

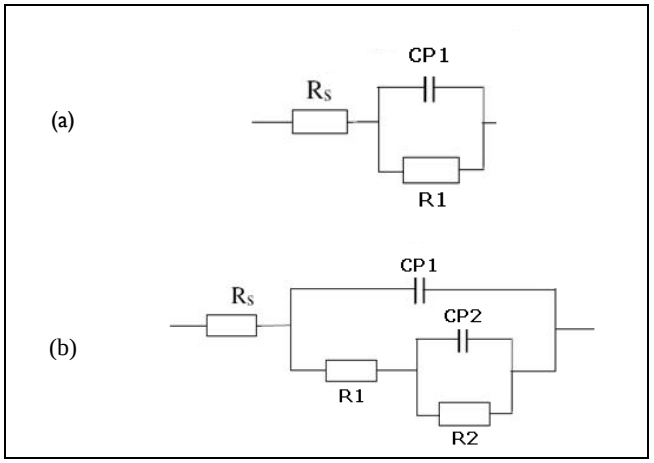


Figure 3. Equivalent circuit. a) Fitting circuit for substratum impedance data. b) Fitting circuit for coating impedance data, with the changes of solutions and number of bilayers.

A small semicircle was obtained for the 4140 (substratum) steel sample which proved to be insignificant when compared to the results for Ti(CN)/TiNb(CN) multilayer coatings.

The model which provided the best fit is that presented in Figure 3a. A time constant connected in parallel with the resistance to the charge transfer, and in series with the resistance of the solution, was observed in this circuit. Two semicircles (Figure 2) were observed when varying the coatings' bilayers (1, 50, 100, 150 and 200); therefore, it was used to model an equivalent circuit having two constant phase elements (CP1 and CP2), represented in Figure 3b. The CP1-R1 elements were present at high frequencies and were associated with the reactions occuring around the passivating surface oxide layer generated by the coatings. A second set of CP2-R2 elements, present at very low frequencies (1 MHz), were associated with the barrier layer generated by the surface oxide layer and the substratum due to the charge transfer; this set of elements represented the response of system processes, which were slow in the coatings obtained.

### *Erosion*

Figure 4 shows the dynamic curves of wear for erosion and 30° impact angle. The curves indicated that the substratum had greater weight loss as time elapsed; due to its greater ductility, it suffered wear proportional to exposure time. However, when applying a Ti(CN)/TiNb(CN) multilayer coating to the substratum, a reduction in the steepness of the curves towards lower weight loss values was obtained as time elapsed, showing the beneficial effect of coating 4140 steel. The Ti(CN)/TiNb(CN) multilayer having 200 bilayers had the lowest losing material value. The samples with Ti(CN)/TiNb(CN) multilayer having 200 and 150 bilayers had a reduction in mass of 83% and 97%, respectively, compared to the uncoated substratum, showing the beneficial effect of the Ti(CN)/TiNb(CN) multilayer system using different bilayers on uncoated steel 4140.

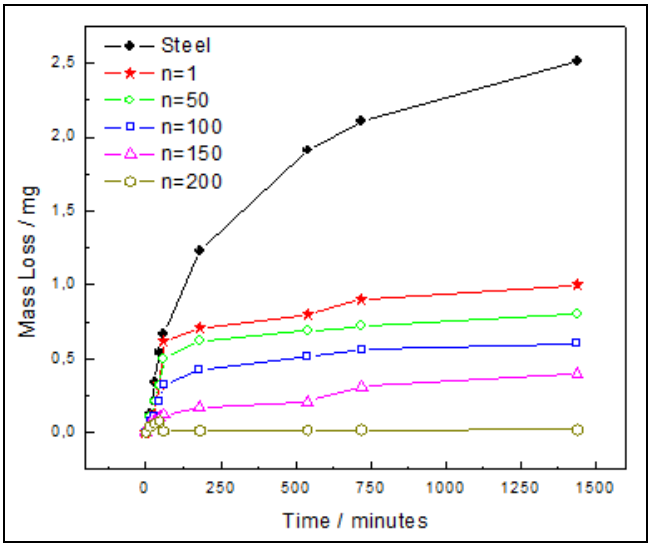


Figure 4. Dynamic erosion wear curves at 30° angle with no corrosive effect

### *Corrosion–erosion*

The Nyquist diagrams shown in Figure 5 displayed a decreased total impedance pattern in each multilayer evaluated, compared to the effect of dynamic corrosion (Table 1). The combined effects of erosion and corrosion resulted in a total loss of material, which was higher than that observed by adding the effects of

each separate process, indicating that there was synergism in both processes. The synergistic component was total damage resulting from corrosion and wear interaction; the combined effects of wear and corrosion caused greater damage than that caused by the additive effects of each other, being more prominent for AISI 4140 and multilayer substratum with one bilayer. By correlating the other multilayers' patterns it was found that the study materials had virtually the same impedance for 50 and 100 bilayer multilayers. Figure 5 also includes the results of a simulation using the electrical circuit shown in Figure 3b, following the same procedure for obtaining parameter values.

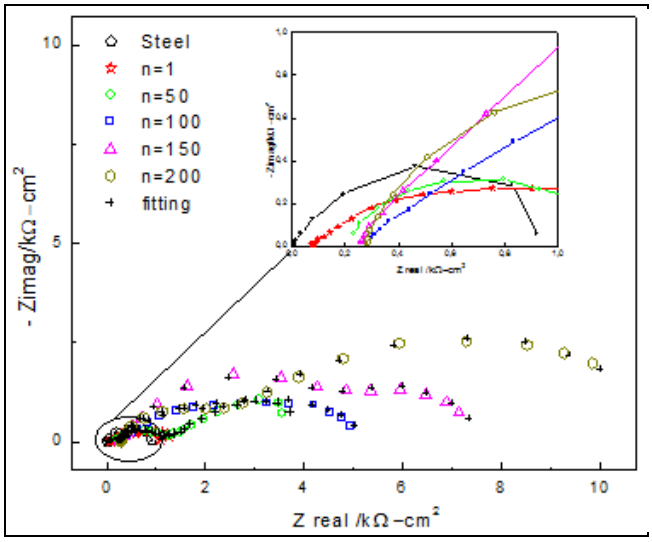


Figure 4. Ti(CN)/TiNb(CN) erosion–corrosion hetero structures impedance diagrams, regarding the number of bilayers

Table 2. Comparing the experimental data for system substratum and coating corrosion erosion to bias variation and the results obtained by Kramers–Kronig relationships (adjustment)

| | $R_\Omega$ $\Omega\ cm^2$ | $CPE_1$ $\mu F\ cm^{-2}\ s^{-(1-\alpha 1)}$ | $\alpha_1$ | $R_1$ $10^3\Omega\ cm^2$ | $CPE_2$ $\mu F\ cm^{-2}\ s^{-(1-\alpha 2)}$ | $\alpha_2$ | $R_2$ $10^3\Omega\ cm^2$ |
|---|---|---|---|---|---|---|---|
| **n=200** | 34.14 (0.3%) | 8.14 (2.1%) | 0.78 (0.2%) | 3.80 (4%) | 45.21 (3%) | 0.82 (0.4%) | 10.24 (2%) |
| **n=150** | 36.2 (0.3%) | 7.42 (1.9%) | 0.69 (0.3%) | 3.56 (2%) | 15.45 (4%) | 0.82 (0.3%) | 4.94 (2%) |
| **n=100** | 35.4 (0.5%) | 6.78 (2.3%) | 0.85 (0.3%) | 2.42 (4%) | 12.32 (2,6%) | 0.89 (0.5%) | 3.65 (3%) |
| **n=50** | 36.2 (0.5%) | 5.45 (3.1%) | 0.87 (0.7%) | 1.37 (6%) | 9.42(1,3 %) | 0.91 (3.1%) | 3.07 (4%) |
| **n=1** | 34.2 (0.6%) | 3.45 (2.4%) | 0.92 (0.5%) | 0.7 (3%) | 6.25(2,3 %) | 0.85 (2.6%) | 1.85 (3%) |
| **Steel** | 32.4 (0.6%) | 2.32 (1.7%) | 0.71 (0.2%) | 1.08 (4%) | | | |

## *Scanning electron microscopy*

Figure 6 shows the micrographs for substratum and multilayer surface having 1, 150 and 200 bilayers after erosion corrosion at 30° impact angle. Figure 6a shows that part of the substratum has been damaged due to the effect of dynamic corrosion; it can be seen how the coating has undergone wear by cracking. Different zones can be distinguished in Figure 6b: the centre of the micrograph shows the harmful effect generated by the action of erosion created by abrasive silica particles' impact energy; however, dark circular areas where the protective effect was lost and the beginnings of pitting corrosion can also be seen. Nonetheless, the protective effect provided by the multilayer system is evident. A central area characterised by the action of corrosion and cracking of the coating produced by abrasive silica particles' impact energy can be distinguished in Figure 6c. Also noticeable in Figure 6d is a homogeneous area of protection generating defence mechanisms in cracking zones and minimal dissolution; these areas had a fracture-free surface representing the protective action afforded by the coatings given by the increasing the number of bilayers.

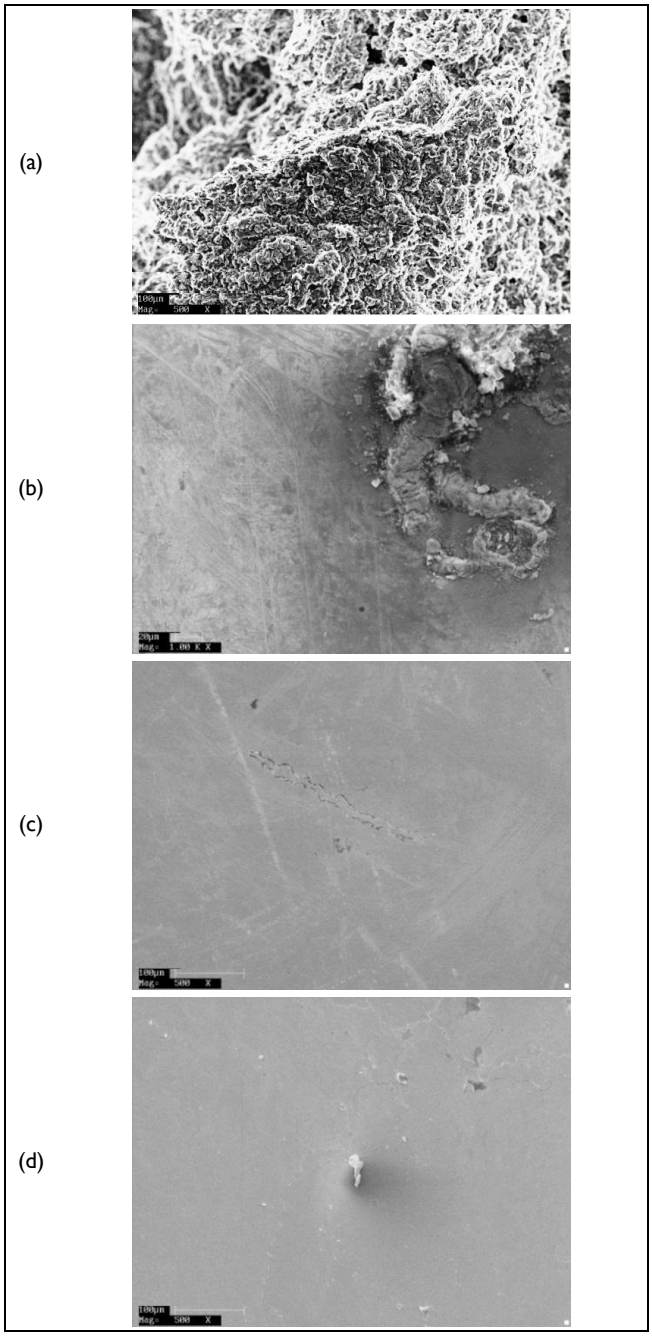


Figure 6. SEM micrograph for samples subjected to corrosion–erosion at 30°. a) substratum; Ti(CN)/TiNb(CN) hetero structures with b) n = 1, c) n = 150, d) n = 200

## Conclusions

The Nyquist diagrams showed good multilayer system performance in dynamic corrosion systems and corrosion-erosion due to the fact that they moved towards areas where polarization resistance became increased, thereby increasing their protection from highly corrosive phenomena.

Multilayer system behaviour in erosion conditions showed that the coatings generated a decrease in material loss and, more meaningfully, to the multilayer system (n=200), i.e. the erosive effect on the multilayer system led to establishing good mechanical properties, generating absorption and distribution of impact energy.

SEM analysis showed that the multilayer system had a protective effect on the substratum when exposed to corrosion-erosion synergy. The harmful effect generated by the action of erosion caused by the abrasive silica particles' impact energy and areas where the protective effect became lost and initiated pitting corrosion was evident in the coated samples.

The erosive effect on the multilayers led to observing an improvement in mechanical properties by generating absorption and distributing impact energy; as the number of bilayers became reduced, mass became lost.

Regarding the erosion-corrosion synergy mechanism, it was evident that mechanical removal of material (substratum and bilayers) through erosion and electrochemical corrosion occurred almost simultaneously.

## Acknowledgements

This work was financed by the Universidad Militar Nueva Granada in Bogotá, Colombia.

## References

Aperador, W., Caicedo, J. C., España, C., Cabrera, G., Amaya, C., Bilayer period effect on corrosion–erosion resistance for [TiN/AlTiN]n multilayered growth on AISI 1045 steel, Journal of Physics and Chemistry of Solids., Vol. 71, No. 12, Dec., 2010, pp. 1754-1759.

Aperador, W., Ramírez-Martín C., Bautista-Ruiz J., Sinergia entre la corrosión erosión del acero 1045 recubierto por multicapas de TiN/TiAlN, Revista Mexicana De Física , Vol. 57, No. 4, Aug., 2011, pp. 350–355.

Barshilia, H. C., Deepthi, B., Rajam, K. S., Bhatti, K. P., Chaudhary, S., Growth and characterization of TiAlN/CrAlN superlattices prepared by reactive direct current magnetron sputtering, Journal of Vacuum Science & Technology A: Vacuum, Surfaces, and Films, Vol. 27, No. 1, Jan., 2009, pp. 29-36.

Barshilia, H. C., Deepthi, B., Selvakumar, N., Jain, A., Rajam, K. S., Nanolayered multilayer coatings of CrN/CrAlN prepared by reactive DC magnetron sputtering., Applied Surface Science, Vol. 253, No. 11, March., 2007, pp. 5076-5083.

Caicedo, J. C., Amaya, C., Yate, L., Aperador, W., Zambrano, G., Gómez, M. E., Alvarado-Rivera, J., Muñoz-Saldaña, J., Prieto, P., Effect of applied bias voltage on corrosion-resistance for TiC1−xNx and Ti1−xNbxC1−yNy coatings, Applied Surface Science, Vol. 256, No. 9, Feb., 2010, pp. 2876-2883.

Caicedo, J. C., Cabrera, G., Aperador, W., Escobar C., Amaya C., Corrosion-Erosion Effect on TiN/TiAlN Multilayers, Journal of materials engineering and performance. DOI: 10.1007/s11665-011-0093-z, Dec., 2011, pp. 1-7.

Helmersson, U., Todorova, S., Barnett, S. A., Sundgren, J. E., Markert, L. C., Greene, J. E., Growth of single-crystal TiN/VN strained-layer superlattices with extremely high mechanical hardness., Journal of Applied Physics, Vol. 62, No. 2, Nov., 1987, pp. 481-485.

Holmberg, K., Matthews, A., Ronkainen, H., Coatings Tribology-contact mechanisms and surface design, Tribology International, Vol. 31, No. 1-3, Jan., 1998, pp. 107–120.

Jehn, H.A. Improvement of the corrosion resistance of PVD hard coating–substrate systems, Surface and Coatings Technology, Vol. 125, No.1–3, Mar., 2000, pp. 212-217.

Junhua, Xu., Geyang, Li., Mingyuan, Gu., The microstructure and mechanical properties of TaN/TiN and TaWN/TiN superlattice films, Thin Solid Films, Vol. 370, No. 1–2, Jul., 2000, pp 45-49.

Koehler, J. S. Attempt to Design a Strong Solid, Physical Review B, Vol. 2, No. 2, Jul., 1970, pp. 547-551.

Orazem, M. E., Tribollet, Bernard, Electrochemical impedance spectroscopy, New Yersey, John Wiley and Sons, Inc., 2008, pp. 255-260.

Philip, C. Y., William D. S., Nanometer scale multilayered hard coatings, Vacuum, Vol. 55, No. 3, Jul., 1999, pp. 179-190.

Romero, J., Esteve, J., Lousa, A., Period dependence of hardness and microstructure on nanometric Cr/CrN multilayers, Surface Coating Technology, Vol. 188-189, Dec., 2004, pp. 338-343.

Shtansky, D. V., Testing and Application, in: Nanostructured Thin Films and Nanodispersion Strengthened Coatings, NATO Series, eds. A.A. Acad. Publ, 2004, pp. 2876–2883.